# First-order reversal curve analysis of spin-transition thermal hysteresis in terms of physical-parameter distributions and their correlations

Radu Tanasa, Cristian Enachescu, and Alexandru Stancu
*"Alexandru Ioan Cuza" University, Faculty of Physics, Iasi, 700506, Romania*

Jorge Linares, Epiphane Codjovi, and Francois Varret
*Laboratoire de Magnetisme et d'Optique, CNRS-UMR 8634, Université de Versailles 78035, France*

Jaap Haasnoot
*Gorlaeus Laboratories, Leiden University, POB 9502, 2300 RA Leiden, The Netherlands*
(Received 5 August 2004; published 24 January 2005)

We investigate the thermal hysteresis of spin-crossover compounds by using the first-order reversal curve (FORC) method. By magnetic measurements we have recorded the FORC data for the pure Fe- and Zn-diluted spin transition system $[Fe_xZn_{1-x}(btr)_2(NCS)_2].H_2O$, where $x$ governs, through cooperative interactions, the width of the thermal hysteresis loop. The wiping-out and congruency properties are obeyed and support the description of the system by independent spin-like domains. The FORC analysis show, for increasing dilution parameter $1-x$, almost monotonous trends: (i) increasing width of the bias distribution, (ii) decreasing width of the coercivity distribution, (iii) increasing correlation between the bias and coercivity distribution. The Preisach distributions finally are expressed in terms of $P(\Delta, J)$, where $\Delta$=energy gap and $J$=intra-domain interaction parameter are the major physical parameter quantities involved in the two-level (e.g., Ising-like) standard description of interacting spin-crossover units. The physical origin of the distributions is discussed and the eventual $\Delta - J$ correlation is determined. The pure compound exhibits a negligible $\Delta - J$ correlation and therefore can be considered as made of independent spin domains. The diluted compounds exhibit a sizeable $\Delta - J$ correlation, which can merely be explained by a small spreading of the composition parameter.

DOI: 10.1103/PhysRevB.71.014431 PACS number(s): 75.75.+a, 75.30.Wx, 75.60.Ej, 64.60.My

## I. INTRODUCTION

Spin transition compounds are a class of inorganic coordination complexes of transition metal ions with $3d^4-3d^7$ electron configurations, namely Fe(II), Fe(III), Co(II), Mn(II), and Ni(II), located in an octahedral ligand field the strength of which induces the competition between spin states.[1] The diamagnetic low spin state (LS) is the ground state at low temperature, while the paramagnetic high spin state (HS) is the stable state at high temperatures, due to its larger entropy.[2] Due to elastic interactions between the spin-crossover molecular units, the entropy-driven spin-crossover may result in a first-order thermal transition occurring with hysteresis. The spin state can be switched as well by pressure (some kbar), magnetic field (typically 40 T, Ref. 3), or irradiation in the visible at low temperature. The switching results in large changes in magnetic, optical, and dielectric[4] properties which are promising for futuristic applications to data recording, such as optical memories.

The relevant parameter which characterizes the macroscopic state of the system is the high spin fraction $n_{HS}$, i.e., the proportion of spin-crossover units in the (HS) state. Microscopic parameters involved in the Ising model are $\Delta$ the energy gap between the spin states of isolated spin-crossover units, $g=g_{HS}/g_{LS}$ the effective[5–9] degeneracy ratio of the spin state (also accounting for the different densities of vibrational states), and $J$ the intra-domain interaction parameter. The equilibrium value of $n_{HS}$ is easily derived from the canonical treatment of the Ising Hamiltonian analysis. The main results of the mean-field treatment are summarized as follows: (i) an equilibrium temperature $T_{1/2}$, at which $n_{HS}=1/2$, is obtained irrespective of the interaction parameter: $k_BT_{1/2}=\Delta/\ln g$; (ii) above a threshold value of the interaction parameter ($J_{thres}=k_BT_{1/2}$ in the mean-field approximation), the spin-crossover occurs with a first-order character. The width of the thermal hysteresis $T_{up}-T_{down}$ is an increasing function of $J$; the mean transition temperature $(T_{up}+T_{down})/2$ remains close to $T_{1/2}$.

In mean-field description, the "effective" interaction in the diluted system is proportional to the number of spin-crossover neighbors, i.e., to the composition parameter $x$. Below a threshold value $x\sim0.40$ the hysteresis loop was observed to collapse in the isostructural systems $[Fe_xM_{1-x}(btr)_2(NCS)_2]\cdot H_2O$ where the dilution metal M was Co or Ni.[10–12]

The present work is devoted to the system $[Fe_xZn_{1-x}(btr)_2(NCS)_2]\cdot H_2O$. The major thermal hysteresis loops, derived from magnetic measurements, are reported in Fig. 1, and the spin state phase diagram in ($x$, $T$) axes is shown in Fig. 2. The threshold value $x\sim0.33$, only is in a qualitative agreement with the Co- and Ni-diluted series data ($x\sim0.38$). The large variation of the mean transition temperature upon the effect of dilution can be explained by the large ionic radius of the Zn(II) ion, which roughly matches the Fe(II) radius in the HS state. Following the steric arguments used in Ref. 10, 11, and 13, the presence of molecular units with a large radius stabilizes the HS state of the spin-crossover units, i.e., lowers the equilibrium temperature (by decreasing $\Delta$).

 

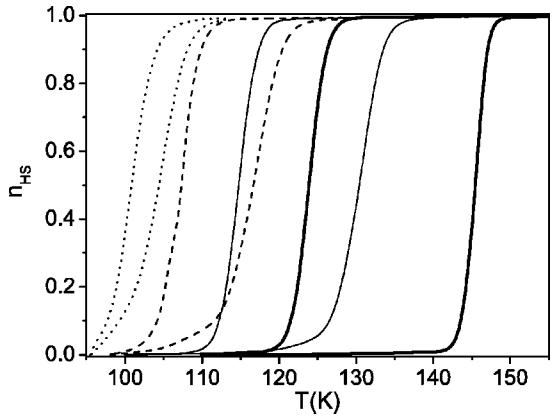


FIG. 1. Thermal hysteresis for $[Fe_xZn_{1-x}(btr)_2(NCS)_2]\cdot H_2O$, with $x=1$ (pure compound), $x=0.8$, $x=0.6$, and $x=0.4$ from right (wider loops) to left (narrower loops), respectively.

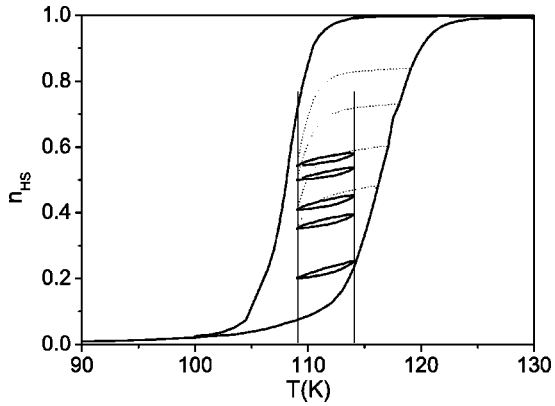


FIG. 3. Minor hysteresis loops of $[Fe_{0.6}Zn_{0.4}(btr)_2(NCS)_2]\cdot H_2O$. The congruency property is observed.

Some time ago, it was suggested that the spin transition occurs through spin-like domains, including molecules in the same spin state, responsible for the capability of exhibiting minor hysteresis loops.[14] Based on this assumption the classical[15] and generalized[16] Preisach model could be applied for analyzing the thermal hysteresis of $[Fe_xCo_{1-x}(btr)_2(NCS)_2]\cdot H_2O$.[13,17] The Preisach plane was of course the $(T_{up}, T_{down})$ plane, instead of the magnetic field switching values for the genuine formalism aiming to analyze the magnetic hysteresis of ferro- (or ferri-) magnetic systems.

It is known that the sufficient and necessary conditions for applying the classical Preisach model[18] are the wiping-out property,[16] correlated with the fact that major hysteresis loop is well defined irrespective of the past history of the system, and the congruency property which expresses that the shapes and areas of all minor loops obtained between the same extreme temperatures are the same, irrespective of the location of the minor loops in the major loop. While the wiping-out property is so far respected by all known thermal transitions, the situation regarding the congruency property is different. Konig *et al.*[19] and Muller *et al.*[20] recorded different minor hysteresis loops of a spin transition compound, between two fixed temperatures and measured identical areas. On the basis of the Everett model[21] they deduced that the spin domains do not interact. The same observation has been made by Constant-Machado *et al.* for the pure spin transition compound $[Fe(btr)_2(NCS)_2]\cdot H_2O$;[13] but it was shown that this assumption was no longer valid for diluted compounds such as $[Fe_xCo_{1-x}(btr)_2(NCS)_2]\cdot H_2O$;[16] in addition, it was shown by microprobe technique that the composition Fe/Co was sizeably inhomogeneous in each crystal of the compound,[12] in agreement with the observed correlation between the mean transition temperature and hysteresis width distributions. The questions of the compositional inhomogeneity of the sample and of the independence of the spin domains are central and will be addressed in the present report.

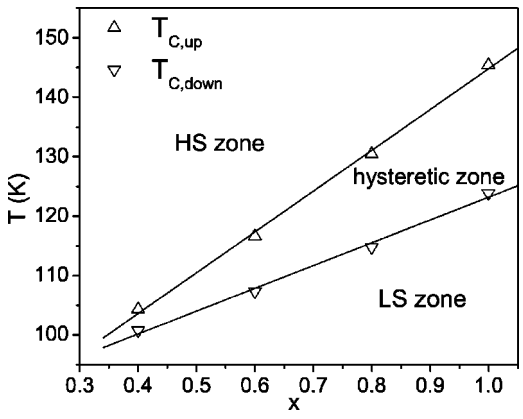


FIG. 2. The dilution-temperature phase diagram of the spin state.

As a preliminary investigation, we measured a series of minor loops for our compound $[Fe_{0.6}Zn_{0.4}(btr)_2(NCS)_2]\cdot H_2O$ between the fixed extreme temperatures 108, 114 K (Fig. 3) and we observed that, in the limit of inherent experimental errors, the congruency property[16] is obeyed, so that the classical Preisach model can be applied.

The FORC method[22] was formerly introduced for analyzing magnetic domains.[23] The FORC analysis of a spin transition was very briefly reported in Ref. 24, and we describe here a more extensive application of the method, aiming to describe the spin-like domain properties in terms of physical quantities such as the energy gap and the intra-domain interaction. Major issues will be the eventual composition distribution and inter-domain interactions. The comparison between magnetic and spin-like domain properties will be briefly addressed.

## II. THE FORC METHOD FOR THERMAL TRANSITIONS

The FORC (first-order reversal curves)[22–24] are a specific class of minor hysteresis loops, for which the sweeping process of the input parameter is reversed only once. For a thermal transition the warming/cooling modes are to be distinguished. The measurements start at a sufficiently high/low temperature, such that the high/low temperature (HS/LS) domain structure is saturated. Then temperature is lowered/raised until a given temperature $T_B$, the reversal temperature, and afterwards raised/lowered, in the warming/cooling

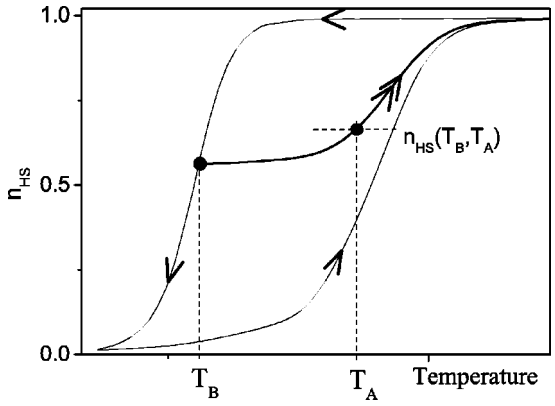


FIG. 4. A FORC curve in the warming mode. Starting for the saturated HS domain state, temperature is lowered (major loop branch) and then raised (FORC data).

mode, respectively, as illustrated in Fig. 4. During the second step of the process, the output parameter (here $n_{\mathrm{HS}}$) is measured as a function of the actual temperature, $T_A$. The experiment is repeated for several values of $T_B$, and the set of $n_{\mathrm{HS}}(T_A,T_B)$ values forms the FORC data.

The FORC distribution is defined as the second derivative of the output parameter (high spin fraction here):

$$\rho(T_A,T_B) = -\frac{\partial^2 n_{\mathrm{HS}}(T_A,T_B)}{\partial T_A \partial T_B}. \tag{1}$$

In the case of non-interacting domains, (e.g., for $x=0.6$, in the present system) the FORC distribution merely is the Preisach distribution, e.g., $P(T_{down},T_{up})$ in the warming mode and $P(T_{up},T_{down})$ in the cooling mode, where $T_{up},T_{down}$ are the switching temperatures of the elementary hysteresis loops (the so-called hysterons of the Preisach formalism). In such a case the FORC distributions obtained in the cooling and warming modes are expected to be the same. The major advantages of the FORC method are: (i) it has a purely analytical character, i.e., it is model-independent, (ii) it rules out the unphysical situation data such as $T_{down}>T_{up}$, i.e., in case of reversible components, $T_{down}=T_{up}$ is really obtained.

On the other hand, the drawback inherent to the "raw" character of the data is the need for additional information for reaching unambiguous conclusions. Fortunately, in the present study, the congruency property gives direct access to the Preisach distribution, and allows unambiguous conclusions to be reached.

## III. EXPERIMENTAL TECHNIQUES AND MEASUREMENTS

The samples were prepared at the Leiden University,[25] as small crystals, in the shape of rectangular platelets, little colored (between white and yellow) at room temperature and turning to dark purple at low temperature. After repeated thermal transitions, self grinding of the crystals occurred and rapidly the sample was in powder state. Such a preliminary treatment, following Refs. 12 and 13 was systematically performed, in order to obtain reasonably reproducible major hysteresis loops. Due to the color change, the spin transition could also be detected by optical measurements. For the present study, we have only used magnetization measurements, made using a superconducting quantum interference device magnetometer (MPMS5 Quantum Design) in the RSO mode. Reflectivity data, which may exhibit some differences with respect to the magnetic data,[26] will be presented in a separate report.

In Fig. 5 we present the experimental FORCs of thin samples of $[Fe_xZn_{1-x}(btr)_2(NCS)_2]\cdot H_2O$ (about 5 mg), derived form the magnetization measurements under applied field 1000 Oe. Temperature was scanned every 0.5 K for both $T_A$ and $T_B$. The high spin fraction was derived from the susceptibility value, considering, respectively, the paramagnetic and diamagnetic characters of the HS and LS states. For $x=0.6$, the measurements were made both in the warming and in the cooling modes and led to slightly different FORC distributions, which will be discussed separately (Sec. VIII).

## IV. EXPERIMENTAL FORC DIAGRAMS

The experimental FORC diagrams, calculated using Eq. (1), are represented in Fig. 6. In order to facilitate the discussion of the results in physical terms, we have chosen the $b=(T_A+T_B)/2$, $c=(T_A-T_B)/2$ axes which roughly correspond to the energy gap $\Delta$ and intra-domain interaction $J$. The corresponding axes for magnetic systems would be the bias and coercivity, respectively. It is worth noting that the centers of the FORC distributions are situated along a straight line, which of course is consistent with the phase diagram already shown in Fig. 2.

A key point is that $\Delta$ is pressure sensitive,[27–29] and therefore can be modulated by internal stresses due to local defects, or by external stresses mediated by the elastic interactions between spin-like domains. This gives rise to a generic difference between the magnetic and spin-crossover systems: the biases in spin-crossover systems cannot be unambiguously attributed to inter-domain interactions. In the present case, since the congruency property is obeyed, such inter-domain interactions are de facto ruled out, and the bias effect has to be exclusively attributed to intra-domain properties. This is a general property of the thermal transitions, because the central value ($T_{1/2}$) of the input parameter of the hysteron is not imposed by symmetry, contrary to magnetic systems which are invariant upon time-reversal. Such a difference is reflected in the models: the true spins of magnetic systems are submitted to true magnetic fields while the fictitious spins of the Ising-like model (the key difference with true Ising model is the degeneracy ratio $g\neq 1$) are submitted to a temperature-dependent fictitious field[30] which goes through zero at a temperature ($T_{1/2}$) which obviously is system-dependent.

The coercivity, associated with the width of the thermal hysteresis loop, is not expected to sensitively depend on internal stresses, since pressure experiments on spin transition compounds[27–29] do not show a rapid variation of the thermal hysteresis width. Coercivity should be related mainly to the dilution parameter (see the phase diagram) and presumably

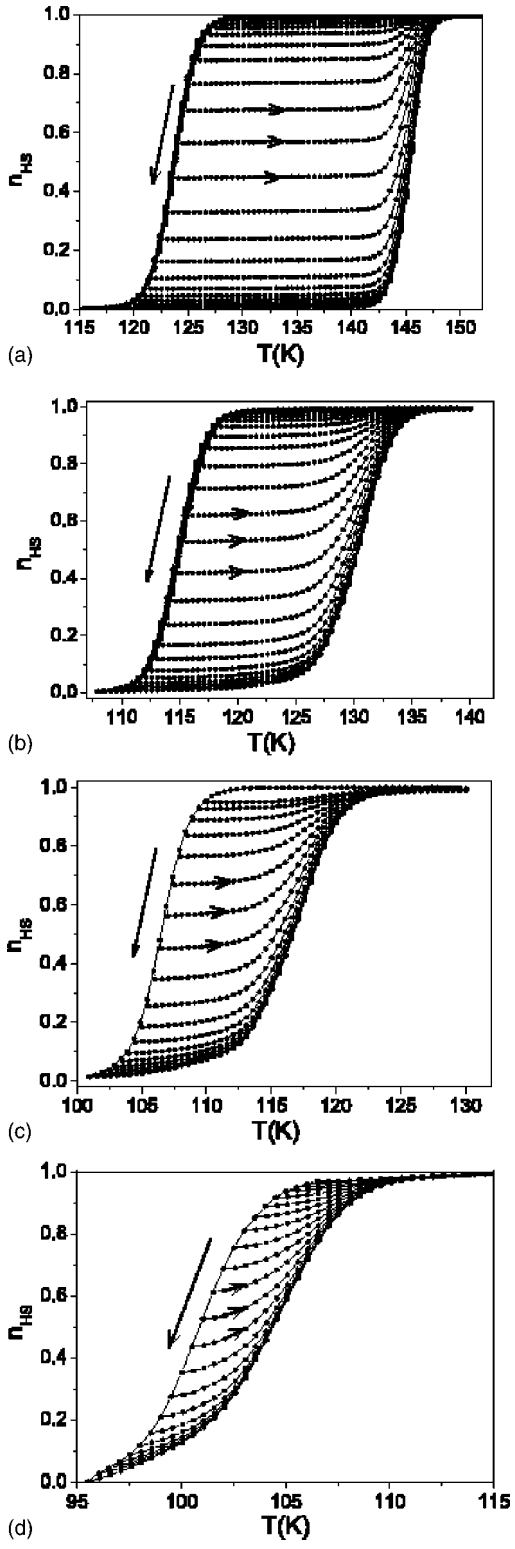


FIG. 5. Experimental FORCs in the warming mode for (a) the pure compound ($x=1$); (b) for $x=0.4$; (c) for $x=0.6$; (d) for $x=0.4$.

to the domain size, according to an intuitive analogy to the dynamic properties of magnetic nano-particles (amazingly, the problem of nano-size spin-transition crystals has not been really addressed so far, to the authors' best knowledge).

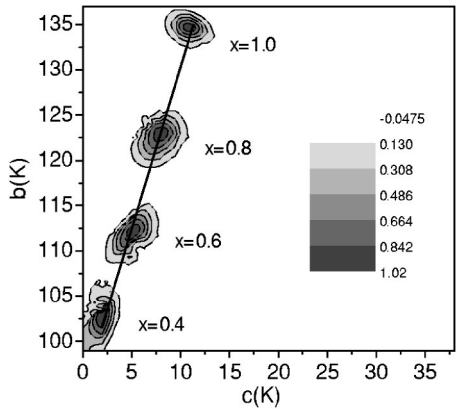


FIG. 6. FORC diagram for different concentrations in the bias-coercivity $(b,c)$ plane.

## V. THE BIAS-COERCIVITY CORRELATION

Before proceeding to the detailed statistical analysis, it is convenient to control the normal character of the distributions. We therefore introduce the separate distributions:

$$P(b_i) = \sum_j P(b_i, c_j), \quad P(c_j) = \sum_i P(b_i, c_j). \tag{2}$$

We show in Fig. 7 some typical data which illustrate the normal character of the experimental distributions. The shapes of all experimental distributions are close to Gaussian, and we have summarized in Table I the application of the usual statistical criterion.

A crucial point for joint probability distributions is the correlation between parameters, quantitatively expressed through the dimensionless coefficient:

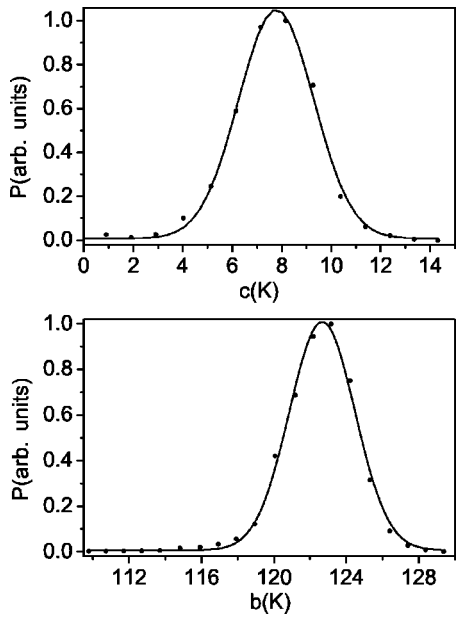


FIG. 7. Experimental bias and coercivity distributions, $P(b)$ and $P(c)$ obtained for $x=0.8$ with fitted Gaussian distributions (parameter values listed in Table I).

TABLE I. The statistical data for the normal character of the experimental distributions, and fitted Gaussian parameters.

| $x$ | $\bar{c}$(K) | $\sigma(c)$(K) | $\chi_c^2$ | $\bar{b}$(K) | $\sigma(b)$(K) | $\chi_b^2$ |
|---|---|---|---|---|---|---|
| 0.4 | 1.63 | 1.13 | 0.0015 | 102.74 | 2.27 | 0.0003 |
| 0.6 | 5.19 | 1.51 | 0.0007 | 113.14 | 1.79 | 0.0012 |
| 0.8 | 7.77 | 1.52 | 0.0005 | 122.66 | 1.81 | 0.0005 |
| 1.0 | 12.84 | 1.99 | 0.0009 | 136.44 | 0.81 | 0.0069 |

$$r(b,c) = \frac{\mathrm{cov}(b,c)}{\sigma(b)\sigma(c)} = \frac{\sum_{ij}(b_i-\bar{b})(c_j-\bar{c})P(b_i,c_j)}{\left\{\left(\sum_{ij}(b_i-\bar{b})^2P(b_i,c_j)\right)\left(\sum_{ij}(c_j-\bar{c})^2P(b_i,c_j)\right)\right\}^{1/2}}, \tag{3}$$

where the summation is performed over all possible values of the parameters: $(b_i>0)$ and $(c_j>0)$ [because $T_A>T_B$].

Due to the normal character of the distributions, the joint probability can be modeled by

$$P(b,c) \sim \exp\left(-\left(\frac{(b-b_0)^2}{2\sigma_b^2}+\frac{(c-c_0)^2}{2\sigma_c^2}-r\frac{(b-b_0)(c-c_0)}{\sigma_b\sigma_c}\right)\right), \tag{4}$$

where $r$ (such as $r^2<1$) merely is the correlation parameter $r(b,c)$ defined by Eq. (3) and $\sigma_b$, $\sigma_c$ are input parameters derived from the standard deviation values $\sigma(b)$, $\sigma(c)$, according to

$$\sigma_b = \sigma(b)\sqrt{1-r^2}, \quad \sigma_c = \sigma(c)\sqrt{1-r^2}. \tag{5}$$

The statistical analysis data of the $P(b,c)$ distributions are collected in Table II, which are slightly distinct form those reported in Table I, due to different calculating algorithm (direct summation). The Gaussian form of Eq. (4) gives the contour plots of the joint distributions elliptical shapes in excellent agreement with the experimental results. The ellipse axes are rotated with respect to the $(c,b)$ axes by an angle $\alpha$ (defined modulo $\pi/2$) expressed through

$$\tan 2\alpha = 2r\frac{\sigma_b\sigma_c}{\sigma_c^2-\sigma_b^2} = 2r\frac{\sigma(b)\sigma(c)}{\sigma(c)^2-\sigma(b)^2}. \tag{6}$$

The pure compound exhibits a negative, but relatively small $(b,c)$ correlation. Diluted systems with increasing Zn content exhibit a larger correlation between bias and coercivity, as shown by the obvious rotation of the contour plots in Fig. 6, as well as by the clear distortion of the major hysteresis loop. The latter effect is illustrated by adequate simulations, in Fig. 8.

A brief discussion of the parameter values leads to the qualitative conclusion that dilution increases the number of local defects responsible for the bias distribution but weakens the average effective interaction, so that finally increasing dilution reduces the coercivity distribution. The positive correlations observed for the diluted compounds can be explained by the effect of a small distribution of the composition parameter $x$, which would tend to expand the $P(b,c)$ contour plots along the line representative of the average phase diagram (straight line in Fig. 6). The quantitative discussion of the correlation requires one to express the distributions in terms of physically relevant parameters, a problem which will be addressed in the next section.

## VI. JOINT DISTRIBUTIONS OF THE RELEVANT PHYSICAL PARAMETERS ($\Delta$,$J$)

We now turn to the description of the joint distributions in terms of relevant physical parameters. Due to the two-dimensional character of the Preisach plane, we have been led to select two physical parameters: the energy gap $\Delta$ and the intra-domain interaction $J$. The degeneracy parameter, correlated to the entropy change upon transition, was discarded in a first approach. Such a choice resulted from the assumption that the distributions were due to internal stresses, which at first approach[27] only affect the energy gap,

TABLE II. The statistical data and distribution input parameters derived from the experimental distributions of bias, $b=(T_A+T_B)/2$ and coercivity, $c=(T_A-T_B)/2$ using direct summation.

| $x$ | $\bar{b}$ (K) | $\sigma(b)$ (K) | $\bar{c}$ (K) | $\sigma(c)$ (K) | $r(b,c)$ | $\sigma_b$ (K) | $\sigma_c$ (K) | $\alpha$ (deg) |
|---|---|---|---|---|---|---|---|---|
| 0.4 | 102.53 | 2.32 | 1.61 | 1.03 | 0.45 | 2.07 | 0.92 | +77 |
| 0.6 | 111.58 | 1.65 | 5.05 | 1.28 | 0.52 | 1.41 | 1.09 | +58 |
| 0.8 | 122.61 | 1.71 | 7.74 | 1.47 | 0.25 | 1.65 | 1.42 | +60 |
| 1.0 | 134.56 | 1.03 | 10.81 | 1.24 | −0.26 | 1.00 | 1.19 | −28 |

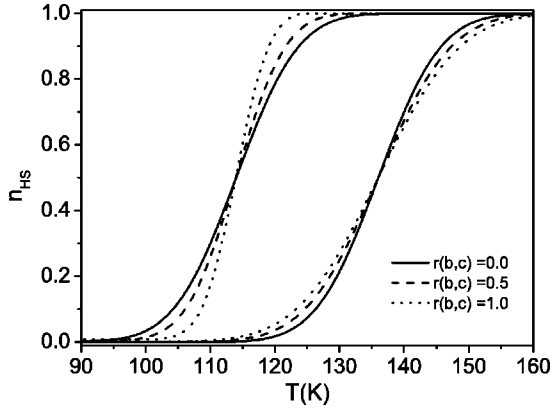


FIG. 8. Set of major hysteresis loops computed using the correlated joint distribution [Eq. (4)], with parameter values: $\sigma_b=7$, $\sigma_c=3$, $r(b,c)=0$, 0.5, 1.

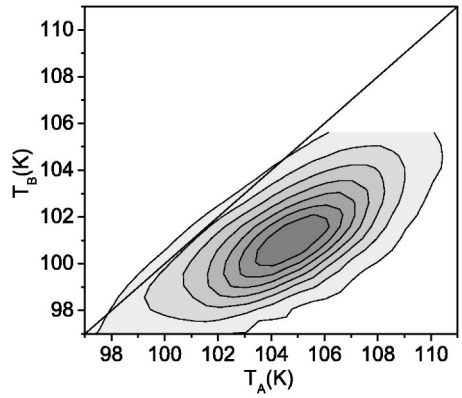


FIG. 10. The FORC diagram of $[Fe_{0.4}Zn_{0.6}(btr)_2(NCS)_2]\cdot H_2O$, determined in the warming mode exhibiting a small reversible component.

and to domain size effects, supposed to act only on the hysteresis width, thus neglecting further effects known to be essential for magnetic nanoparticles, such as surface effects.[31]

We use here the Ising-like model, introduced in Ref. 5 for spin-transitions. Each spin-crossover molecular unit is represented by a fictitious spin, a two-level operator with energy gap $\Delta=\Delta H/R=E_{\mathrm{HS}}-E_{\mathrm{LS}}>0$, and degeneracy ratio $g=\exp(\Delta S/R)=g_{\mathrm{HS}}/g_{\mathrm{LS}}\gg 1$.

The Ising-like Hamiltonian can be written in a "true" Ising equivalent form (degeneracy ratio $=1$) by considering a temperature dependent energy gap,[6] i.e., a fictitious effective field written $\Delta_{eff}=\Delta-k_BT\ln g$, acting on the fictitious spins. At $T_{1/2}$, $\Delta_{eff}=0$.

Straightforward canonical treatment of the Ising-like model, in mean-field approximation, was performed in order to derive the relationships $T_A=f(\Delta,J,g)$, $T_B=f(\Delta,J,g)$. The data computed for a given $g$ value have been plotted in Fig. 9. According to the calorimetric data of the system[12] the relevant $g$ values are: $g=8000$ ($x=1$), $g=4000$ ($x=0.8$), $g=2000$ ($x=0.6$), $g=1000$ ($x=0.4$). It should be kept in mind that the shapes of the hysteresis loops computed in the mean field approximation usually depart from the experimental shapes. However, in most cases the experimental loop is nearly square-shaped (see Refs. 30 and 32 for a discussion and models beyond the mean-field approximation), and support the recourse to the square hysterons involved in the Preisach analysis.

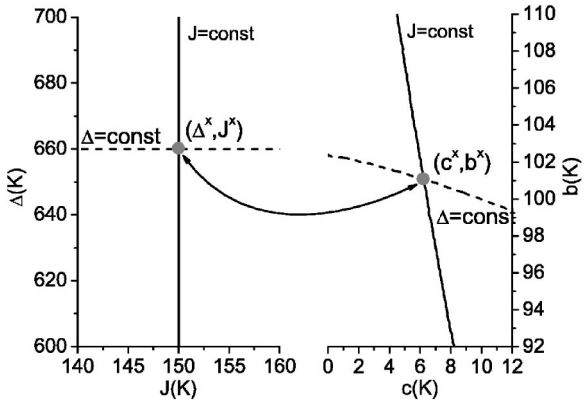


FIG. 9. The bi-univocal correspondence between the $(\Delta,J)$ and $(b,c)$ planes, computed for the degeneracy ratio $g=1000$, illustrated by the intersect of the curves $J=J^x$ (solid line) and $\Delta=\Delta^x$ (dashed line).

It is clear from Fig. 9 that the correspondence between the $(\Delta,J)$ plane, restricted to $J>\Delta/\ln g$, and the bias-coercivity plane, $(b,c)$, is bi-univocal. This is obviously true for the $(T_A,T_B)$ plane, restricted to $T_A>T_B$. The transformation of the joint distributions is straightforward using the Jacobian transformation:

$$P(\Delta,J)=P(T_A,T_B)\left|\frac{\partial(T_A,T_B)}{\partial(\Delta,J)}\right|=P(b,c)\left|\frac{\partial(b,c)}{\partial(\Delta,J)}\right|, \quad (7)$$

where the Jacobian values $|\partial(T_A,T_B)/\partial(\Delta,J)|=2|\partial(b,c)/\partial(\Delta,J)|$ are numerically derived from the set of computed data used for Fig. 9.

It is worth noting that the reversible part of the Preisach distributions does not fulfill the condition $T_A>T_B$. In other words in absence of hysteresis the model fails. Such a situation occurred with the most diluted sample ($x=0.4$), see Fig. 10, the small reversible contribution of which was dropped when determining $P(\Delta,J)$.

The calculated distributions in the $(\Delta,J)$ plane are reported in Fig. 11. The statistical parameters associated with the joint probability densities $P(\Delta,J)$ are listed in Table III. The statistical criterion we used for testing the independence of the random $(\Delta,J)$ variables was defined as $\chi^2_{indep}=\Sigma_{i,j}(o_{ij}-e_{ij})^2/e_{ij}$, where $o_{ij}$ is observed value and $e_{ij}$ is expected value. The probability $P_{indep}$ for $(\Delta,J)$ to be independent is derived from the $\chi^2_{indep}$ value, accounting for degrees of freedom of the problem (here : 504= number of independent data), according to statistical tables from Ref. 33. This probability is found to be high for the pure compound, and low for the diluted compounds. Consequently: (i) the $(\Delta,J)$ parameters are not correlated in the pure compound, so the distribution shall be assigned to different physical processes. The small negative value of the bias-coercivity correlation is explained by a generic property of the two-level system,

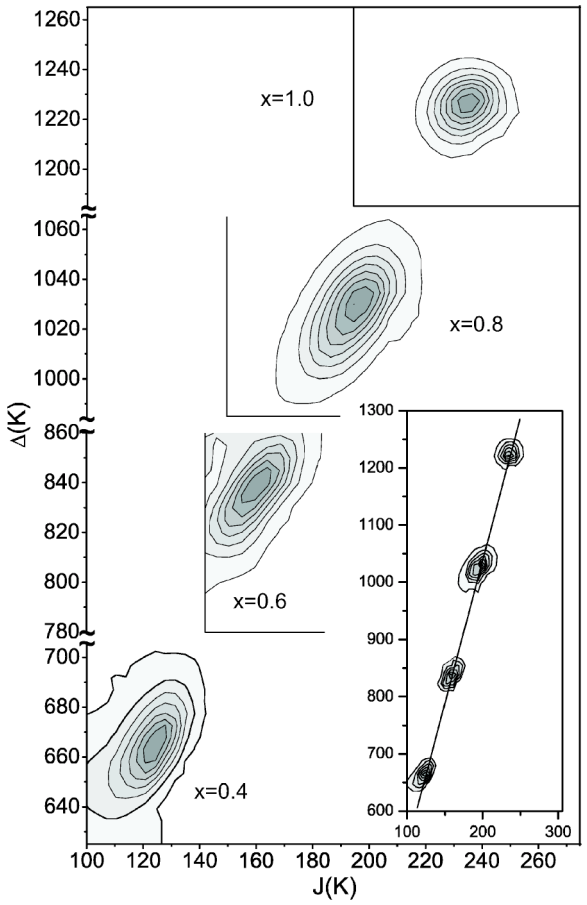


FIG. 11. The $P(\Delta,J)$ distributions of the system $[Fe_xZn_{1-x}(btr)_2(NCS)_2].H_2O$, $x=1$, 0.8, 0.6, 0.4, determined from the FORC data in the warming mode.

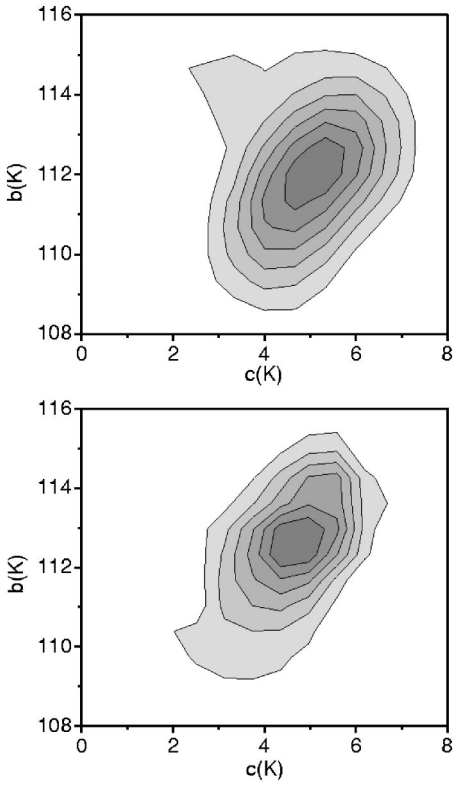


FIG. 12. FORC diagrams for $x=0.6$ in the cooling (top) and warming (bottom) modes.

which states that, at constant $J$ and $g$, coercivity is a decreasing function of the transition temperature (it even vanishes at a critical temperature[30]); (ii) in the present study, the $(\Delta,J)$ correlation is tightly associated with the dilution of the compound.

## VII. DISCUSSION: AN ADDITIONAL COMPOSITION DISTRIBUTION

Upon dilution the spreading of energy gaps $\Delta$ increases at once, while the spreading of interaction parameter $J$ first increases and then decreases. These simple conclusions of course agree with the previous observations concerning the bias and coercivity distributions.

More informative is the discussion concerning the $\Delta-J$ correlation, which is obviously associated with the diluted state of the system. A single glance to Fig. 11 shows a common orientation of the contour plots along the curve representing the variation of mean properties of the system as a function of dilution, i.e., the $\Delta-J$ line derived from the mean $b-c$ line in Fig. 6. The simple idea of a sizeable spreading of the dilution parameter obviously follows, as indeed it already was experimentally observed in the isostructural Co-diluted system.[13]

We now introduce the possible spreading of the composition parameter. Due to the congruency property, the system is represented by independent domains, each of them characterized by the set of $(x,\Delta,J)$ values. For a given $x$ value, the central values of the uncorrelated $\Delta-J$ distribution are gov-

TABLE III. The statistical data derived from the experimental distributions $P(\Delta,J)$; $\chi^2$ and $P_{indep}$ are the criterion and statistical probability for the $\Delta-J$ independence; $\sigma_x$, $\sigma_\Delta$, $\sigma_J$ refer to the model developed in Sec. VII. The value $x\sim0.008$ reported for the pure compound illustrates the statistical inaccuracy of the data.

| $x$ | $\bar{\Delta}$ (K) | $\sigma(\Delta)$ (K) | $\bar{J}$ (K) | $\sigma(J)$ (K) | $r(\Delta,J)$ | $\chi^2_{indep}$ | $P_{indep}$ | $\sigma_x$ (K) | $\sigma_\Delta$ (K) | $\sigma_J$ (K) | $\sigma_J/\bar{J}$ |
|---|---|---|---|---|---|---|---|---|---|---|---|
| 0.4 | 665 | 13.9 | 123 | 8.0 | 0.62 | 2563 | $<0.001$ | 0.020 | 10.9 | 6.3 | 0.051 |
| 0.6 | 836 | 13.2 | 159 | 10.2 | 0.79 | 2603 | $<0.001$ | 0.025 | 8.1 | 6.2 | 0.039 |
| 0.8 | 1028 | 14.5 | 195 | 10.4 | 0.56 | 2970 | $<0.001$ | 0.021 | 12.0 | 8.6 | 0.044 |
| 1.0 | 1225 | 8.8 | 235 | 8.3 | 0.16 | 192 | $>0.999$ | 0.0008 | 8.7 | 8.2 | 0.035 |

TABLE IV. The statistical data for $x=0.6$, comparison of the warming and cooling modes.

| $x$ | $\bar{\Delta}$ (K) | $\sigma(\Delta)$ (K) | $\bar{J}$ (K) | $\sigma(J)$ (K) | $r(\Delta,J)$ | $\chi^2_{indep}$ | $P_{indep}$ | $\sigma_x$ (K) | $\sigma_\Delta$ (K) | $\sigma_J$ (K) | $\sigma_J/\bar{J}$ |
|---|---|---|---|---|---|---|---|---|---|---|---|
| 0.6 | 836 | 13.2 | 159 | 10.2 | 0.79 | 2603 | $<0.001$ | 0.025 | 8.1 | 6.2 | 0.039 |
| $0.6_{cooling}$ | 841 | 12.0 | 157 | 9.3 | 0.59 | 2085 | $<0.001$ | 0.019 | 9.7 | 7.5 | 0.048 |

erned by the phase diagram. The joint probability, assuming Gaussian distributions, is expressed as follows:

$$P(\Delta,J,x) \sim \exp\left(-\left(\frac{(x-x_0)^2}{2\sigma_x^2}+\frac{(\Delta-\Delta_0)^2}{2\sigma_\Delta^2}+\frac{(J-J_0)^2}{2\sigma_J^2}\right)\right). \tag{8}$$

where the functions $\Delta_0(x)$, $J_0(x)$ follow the average $\Delta-J$ line drawn in Fig. 11. Straightforward analytic calculations based on the Gaussian expression of the $P(x,\Delta,J)$ joint probability enable calculating the $\Delta-J$ correlation resulting from $\sigma_x$, once $\sigma_\Delta$, $\sigma_J$ and the slopes $\beta=d\Delta_0/dx$, $\gamma=dJ_0/dx$ are known,

$$\sigma(\Delta)=\sqrt{\sigma_\Delta+\beta^2\sigma_x^2}, \quad \sigma(J)=\sqrt{\sigma_J+\gamma^2\sigma_x^2},$$

$$r(\Delta,J)=\frac{\beta\gamma\sigma_x^2}{\sigma(\Delta)\sigma(J)}. \tag{9}$$

In other words, once the statistical values $\sigma(\Delta)$, $\sigma(J)$, $r(\Delta,J)$ have been measured, and using $\beta\sim930$ K, $\gamma\sim190$ K the standard deviation $\sigma_x$ values are immediately derived. The complete sets of parameter values are reported in the right three columns of Table III.

Obviously, i.e., according to the shapes of the major hysteresis loops, the Zn- diluted system exhibits a small spreading of the composition parameter, compared to that of the Co systems. This is possibly due to the ionic radius of Zn(II), which exactly matches that of the Fe(II) in the HS state, and allows the room-temperature crystal growth of the mixed system to occur in the best steric conditions.

Once accounting for the composition distribution, the "intrinsic" $\sigma_\Delta$ values of the diluted compounds show a reduced increase with respect to that of the pure compound. It is concluded that presumably dilution induces structural defects which specifically contribute to the spreading of the physical parameters. This conclusion is supported by the second "intrinsic" spreading parameter, considered in relative value, $\sigma_J/J$, which is observed to increase for increasing dilution. The latter effect can be explained by an increased spreading of domain sizes, associated with the increased dilution; such an effect might be enhanced on approaching the collapse threshold of the hysteresis loop. However, as already said, the size effects remain so far speculative in the field of spin-crossover solids.

## VIII. COMPARISON OF WARMING AND COOLING MODES

The FORC distributions obtained in the warming and in the cooling modes, for $x=0.6$, are shown in Fig. 12; the results of the statistical analysis are reported in Table IV. The two distributions are not equivalent, in clear disagreement with the congruence property. The sizeable difference in the correlation parameter values is related to the difference in the shapes of the major hysteresis loops. Of course such a difference cannot be assigned to different composition spreadings, in other words the differences in $\sigma_x$ values listed in Table IV should not be considered as significant. At the present time, we presumably assign such an effect to a structural effect, probably associated with interplay between the spin transition and a structural transition in the pure $[Fe(btr)_2(NCS)_2]\cdot H_2O$ system, inferred from pressure investigations[28,29] and which might be responsible for the systematic shifts of the major hysteresis loop reported since the previous works[10–12] upon repeated thermal cycling through the spin transition.

## IX. CONCLUSION

To summarize, the FORC approach has proved to be tractable in the case of spin-crossover solids. Experimental data on the system under study are consistent with the very simple picture of independent spin-like domains characterized by their equilibrium temperature and internal interaction parameter. In the diluted system, a narrow distribution of composition can explain the observed correlation between equilibrium temperatures and internal interaction parameters.

## ACKNOWLEDGMENTS

This work was partially supported by the "Programme d'action integree (PAI) franco-roumaine Brancusi," by a NATO Cooperative Linkage Grant between the groups of Iasi and Versailles and by the Romanian government, which sponsored a three month visit for R.T. to the Universite de Versailles. Acknowledgements are due to Dr. Hab. K. Boukheddaden, and Dr. Hab. H. Spiering for fruitful discussions. R.T. and A.S. are indebted to Romania CNCSIS (Grants TD, A) and CERES programs.

[1] P. Gutlich, A. Hauser, and H. Spiering, Angew. Chem., Int. Ed. Engl. **33**, 2024 (1994).
[2] C. P. Slichter and H. G. Drickamer, J. Chem. Phys. **56**, 2142 (1972).
[3] A. Bousseksou, N. Negre, M. Goiran, L. Salmon, J.-P. Tuchagues, M.-L. Boillot, K. Boukheddaden, and F. Varret, Eur. Phys. J. B **13**, 451 (2000).
[4] A. Bousseksou, G. Molnar, P. Demont, and J. Menegotto, J. Mater. Chem. **13**, 2069 (2003).
[5] J. Wajnsflasz and R. Pick, J. Phys. Colloq. **32**, C1 (1971).
[6] S. Doniach, J. Chem. Phys. **68**, 11 (1978).
[7] A. Bousseksou, J. Nasser, J. Linares, K. Boukheddaden, and F. Varret, J. Phys. I **2**, 1381 (1992).
[8] A. Bousseksou, H. Constant-Machado, and F. Varret, J. Phys. I **5**, 747 (1995).
[9] F. Varret, S. Salunke, K. Boukheddaden, E. Codjovi, C. Enachescu, and J. Linares, C.R. Acad. Sci., Ser. IIc: Chim Ser. IIc **6**, 385 (2003).
[10] J.-P. Martin, J. Zarembowitch, A. Dworkin, J. Haasnoot, and E. Codjovi, Inorg. Chem. **33**, 2617 (1994).
[11] J.-P. Martin, J. Zarembowitch, A. Bousseksou, A. Dworkin, J. Haasnoot, and F. Varret, Inorg. Chem. **33**, 6325 (1994).
[12] H. Constant-Machado, J. Linares, F. Varret, J. Haasnoot, J.-P. Martin, J. Zarembowitch, A. Dworkin, and A. Bousseksou, J. Phys. I **6**, 1203 (1996).
[13] H. Constant-Machado, A. Stancu, J. Linares, and F. Varret, IEEE Trans. Magn. **34**, 2213 (1998).
[14] M. Sorai, Y. Maeda, and H. Oshio, J. Phys. Chem. Solids **51**, 941 (1990).
[15] F. Preisach, Z. Phys. **94**, 277 (1935).
[16] I. Mayergoyz, *Mathematical Models of Hysteresis* (Springer, New York, 1991).
[17] C. Enachescu, H. Constant-Machado, N. Menendez, E. Codjovi, J. Linares, F. Varret, and A. Stancu, Physica B **306**, 155 (2001).
[18] I. D. Mayergoyz, Phys. Rev. Lett. **56**, 1518 (1986).
[19] E. Konig, B. Kanellakopulos, B. Powietzka, and J. Nelson, J. Chem. Phys. **99**, 9195 (1993).
[20] E. Muller, S. H, and P. Gutlich, J. Chem. Phys. **19**, 1439 (1983).
[21] D. H. Everett and W. I. Whitton, Trans. Faraday Soc. **48**, 749 (1952).
[22] C. R. Pike, A. P. Roberts, and K. L. Verosub, J. Appl. Phys. **88**, 967 (2000).
[23] A. Stancu, C. R. Pike, L. Stoleriu, P. Postolache, and D. Cimpoesu, J. Appl. Phys. **93**, 6620 (2003).
[24] C. Enachescu, R. Tanasa, A. Stancu, E. Codjovi, J. Linares, and F. Varret, Physica B **343**, 15 (2004).
[25] W. Vreugdenhil, S. Gorter, J. G. Haasnoot, and J. Reedijk, Polyhedron **4**, 1769 (1990).
[26] E. Codjovi, W. Morscheidt, J. Jeftic, J. Linares, M. Nogues, A. Goujon, O. Roubeau, H. Constant-Machado, A. Desaix, A. Bousseksou, *et al.*, ICMM'98 (Seignosse, France), Mol. Cryst. Liq. Cryst. Sci. Technol., Sect. A **335**, 1295 (1999).
[27] J. Jeftic and A. Hauser, J. Phys. Chem. B **101**, 10262 (1997).
[28] E. Codjovi, N. Menendez, J. Jeftic, and F. Varret, C.R. Acad. Sci., Ser. IIc: Chim **4**, 181 (2001).
[29] G. Levchenko, V. Ksenofontov, A. Stupakov, H. Spiering, Y. Garcia, and P. Gutlich, Chem. Phys. **277**, 125 (2002).
[30] K. Boukheddaden, I. Shteto, B. Hoo, and F. Varret, Phys. Rev. B **62**, 14806 (2000).
[31] D. A. Garanin and H. Kachkachi, Phys. Rev. Lett. **90**, 065504 (2003).
[32] J. Linares, C. Enachescu, K. Boukheddaden, and F. Varret, Polyhedron **22**, 2453 (2003).
[33] I. Stegun and M. Abramowitz, *Handbook of Mathematical Functions with Formulas, Graphs, and Mathematical Tables* (Dover, New York, 1965).